Chapter 7

PLANETARY INTERIORS

7.1 The Advantages of Geophysics

The present understanding of the structure and evolution of the Moon depends heavily on the program of geophysical measurements carried out during the Apollo missions. Geophysical measurements have the advantage that many of the parameters can be established by instruments in orbit as well as from those landed on planetary surfaces. Sample return is a useful but secondary part of the geophysics program, enabling the direct measurements of magnetic properties, thermal conductivities, bulk density and so on. Most of our present knowledge of planetary bodies other than the Moon, and Mars to a very minor extent, is based on the assessment of the geophysical data.

Gravity and magnetic measurements acquired from orbiting spacecraft can provide information not otherwise obtainable about planetary interiors. Magnetic measurements may provide evidence of the past history of a planet. Precise measurements of the gravitational field provide constraints on such fundamental properties as the moment of inertia, a basic parameter whose measurement was "eagerly awaited by aficionados of the moon for some 200 years" [1]. However, one must also recall the lament of Lambeck [2] that "it is rather curious and unfortunate that some of the most readily observed geophysical quantities are also the most tantalizing, but ambiguous ones."

7.2 Radii, Densities and Moments of Inertia

Current values for these parameters are given in Table 7.1. The precise determination of radii has allowed accurate mapping of the elevation of planetary surfaces by spacecraft. The circular maria on the Moon are filled to varying depths with lavas, but generally lie at lower elevations than the

irregular maria, which do not occupy deep basins. The far-side highlands are exceedingly rough, but the mare surfaces are smooth, with differences in elevation of only ±150 m over hundreds of kilometers [3]. In general, there is little evidence of sagging of the lavas in the centers of the circular maria. The lava surfaces are remarkably flat, although local subsidence by normal faulting occurs (e.g., in Crisium). Information from the laser altimeters led to the mapping of ancient ringed basins on the lunar far side originally photographed by Russian spacecraft [4, 5]. Detailed surface elevations on both Venus and Mars have also been obtained, allowing, for Venus, our first detailed understanding of the surface topography of that planet [6] (see Section 2.7).

The coefficient of moment of intertia is critical for understanding the density distribution in the lunar interior. The current value of 0.391 ± 0.002 for the Moon indicates that, in addition to a low density crust, it is probably necessary for an increase in density to occur in the deep interior. This may occur in three ways: (a) a primitive iron-rich interior with only the upper half of the Moon differentiated, (b) phase changes to denser minerals such as garnet at depth, and (c) whole-moon melting and formation of an Fe or FeS core. The first two alternatives encounter various difficulties. Melting the outer half of the Moon, leaving a primitive unmelted deep interior, is probably not sufficient to provide a thick enough feldspathic crust (Sections 5.11.3 and 8.4.2). No evidence of garnet signatures is observed in the REE patterns of mare basalts, which may be derived from depths of 400–500 km accordingly (Section 6.5.2). Initial melting and fractionation (removing garnet constituents Ca and Al into the plagioclase-rich crust) probably extended to greater depths and the possibility of a garnet-rich interior is thus diminished. Accordingly, the third alternative of a core is favored [7].

Tolerances in lunar core densities corresponding to an uncertainty of ±0.0025 in the coefficient of moment of inertia are equivalent to about 4.2 g/cm^3 for lunar cores 300 km in radius; hence core compositions of either Fe or FeS are allowable. The alternative of density changes with depth due to initial heterogeneities appears unlikely in view of the evidence for large scale melting of the Moon. In both the Earth and Mars, the values of the coefficient of moment of inertia clearly indicate the existence of a core. The values for Venus and Mercury are not known, but other evidence suggests differentiation and core formation [8, 9].

7.3 Lunar Center of Mass/Center of Figure Offset

The center of mass of the Moon (CM) is displaced from its center of figure toward the Earth (CF) by about 2 km [10]. Three explanations have been forthcoming, and are presented below in order of increasing credibility:

(a) Mare basalt flows are more dense than the crust. They are common on the near side, but less so on the far side. Their volume is insufficient, however, by about an order of magnitude, to account for the offset.

(b) A lunar core might be displaced from the center of mass [11]; however, this model is unrealistic since the displacement would create shear stresses which could not be supported by the hot interior [12]. A variation of this model calls for mantle asymmetry developed as a consequence of crystallization of the magma ocean [13]. In this model, more rapid crystallization of the magma ocean on the far side results in a greater thickness of Mg-rich (low density) cumulates in the far-side mantle. It seems unlikely that such irregularities could persist during magma ocean crystallization or be maintained during cooling if whole-moon melting occurred. All such models are subject to stress relaxation in the high temperature interior unless maintained by convection which could then account for the offset. In addition, the geochemical evidence indicates that any initial heterogeneities due to accretion which might account for the offset were smoothed out.

(c) The conventional explanation is that the far-side highland crust is thicker [10]. It is massive enough, comprising about 10% of the volume of the Moon, and sufficiently irregular in density and thickness to account for the observed center of mass/center of figure offset [3, 14].

Various other suggestions, such as movement of basalt magma from the lunar interior or removal of near-side crust relative to the far side by asymmetric bombardment [15], have not been generally accepted. An important effect arises from this displacement of the center of figure from the center of mass (Fig. 7.1). A particular equipotential surface will be closer to the lunar surface on the Earth-facing hemisphere. Multi-ring basins and craters on this face will flood with lava much more readily than those on the farside for a given depth of melting. The diversity of lunar basalt compositions indicates many different source regions, probably at differing depths, but in general, it is more difficult for lavas to reach the surface on the farside.

7.4 Gravity

The gravity field of the Earth and planets, and the problems of and interpretations possible from the data, are discussed in an extensive review by Phillips and Lambeck [16].

7.4.1 Lunar Gravity

Estimating the lunar gravity field is not a straightforward process for a number of reasons, not the least of which is the paucity of far-side spacecraft

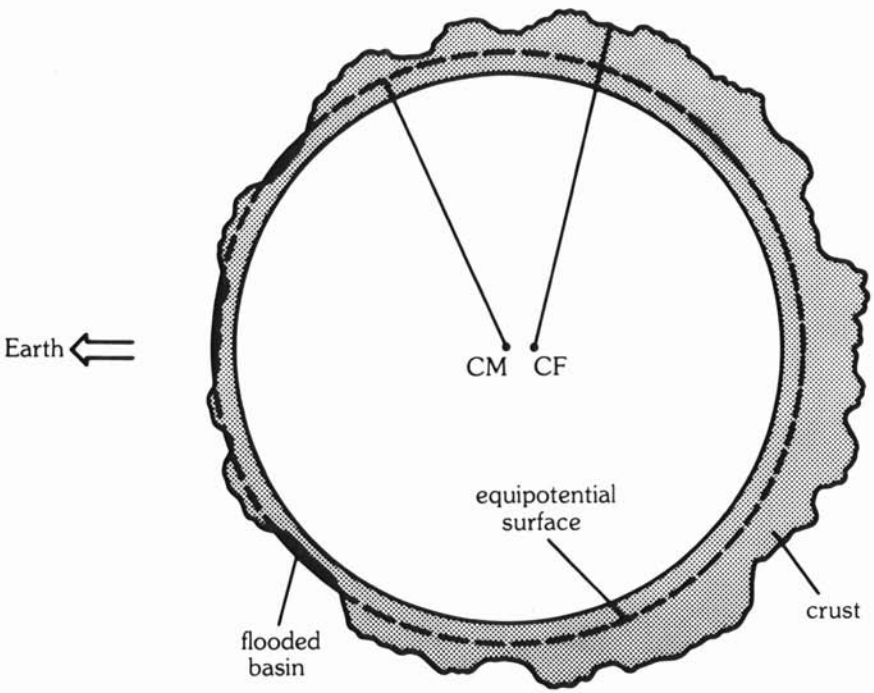

7.1 Cross-section through the Moon in the equatorial plane showing the displacement of the center of mass towards the Earth relative to the center of figure. This is to illustrate that a given equipotential surface will be closer to the lunar surface on the near side than on the far side. Magmas originating at equal depths below that surface will have greater difficulty in appearing as surface lavas on the far side. (Courtesy Susan Pullan.)

tracking data. The lunar gravity field possesses many interesting features, the most notable of which are the mascons, whose discovery in 1968 [17] caused much interest in the state of stress of the lunar crust and the length of time for which it could support such loads.

The early crust appears to be generally compensated, and no effects are discernible from the pre-4.2 billion year bombardment. Formation of the highland crust by flotation in a magma ocean is consistent with this gravity picture. By about 4 aeons the crust had become thick enough and the interior cool enough to support substantial loads for the next 4 billion years. Thus, contrary to earlier interpretations, the Apennine Mountains, which rise 7 km above the present surface of Mare Imbrium, are uncompensated [18]. This provides additional evidence for a relatively cool lunar interior, and that crystallization of the magma ocean was complete by 4.4 aeons. An extensive

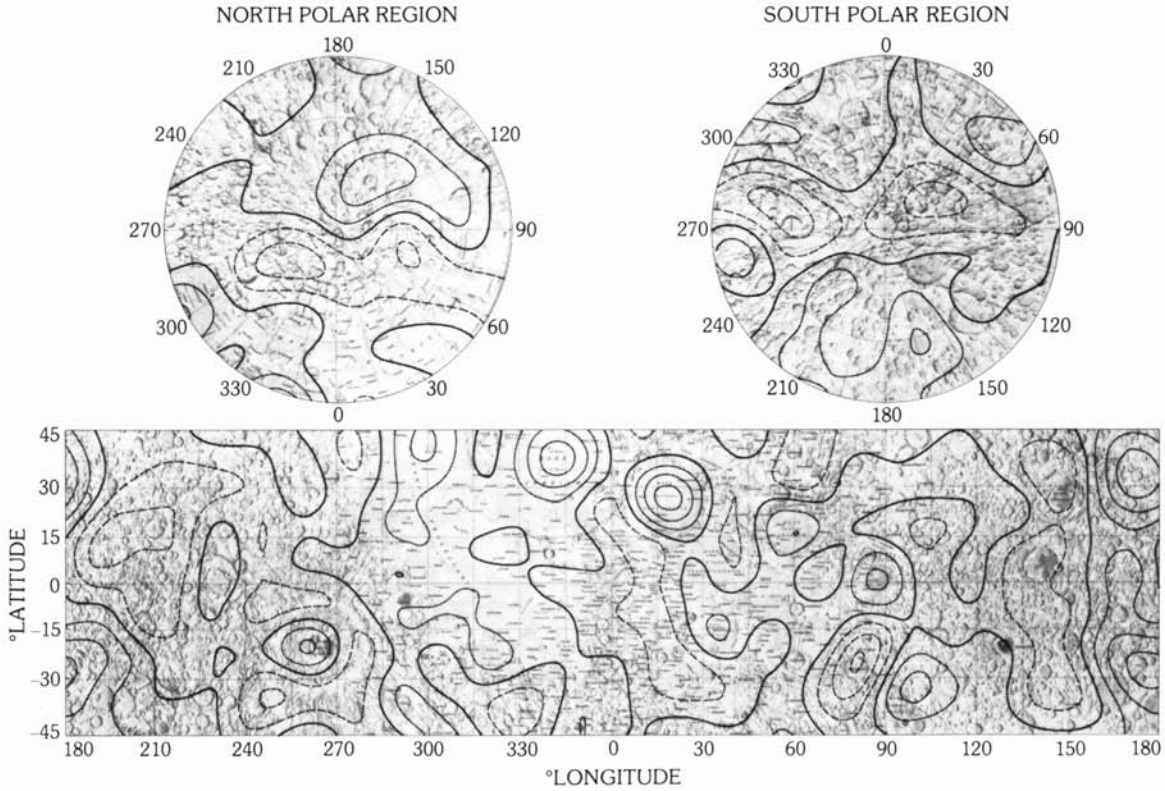

7.2 Lunar Bouguer gravity anomalies. The heavy solid curve is the zero contour. Light solid curves show positive anomalies. Dashed curves indicate negative anomalies. The contour interval is 100 mgal [19]. (Reproduced from *JGR*. 85: 1022, Fig. 7; Courtesy A. J. Ferrari and B. G. Bills).

period of KREEP volcanism in the highlands, with shallow sources implying high near surface temperatures, at about 4.0 aeons must be judged unlikely. (The view is taken throughout this book that the source of KREEP is related to the final stages of crystallization of the magma ocean at about 4.4 aeons. Younger "KREEP basalts" are interpreted as impact melts.) The subsequent partial melting in the deep interior to produce mare basalts between about 4.0 and 3.0 aeons had no effect on the strength of the crust and upper lithosphere, since the observed volume of basalt produced is about only 0.1% of total lunar volume.

The most spectacular Bouguer gravity anomalies are displayed by the Orientale Basin (Fig. 7.2), which has a "bull's eye" appearance, with a central positive region (+200 mgal) surrounded by a ring of negative anomaly (−100 mgal) with an outer positive apron (+30 to +50 mgal). These conclusions, although based on limited data, are firm. Orientale had only restricted coverage during the missions, and for this reason, the topography is not well constrained. With the exception of Orientale and the other mascons, the lunar gravity field is mild with variations typically of ±30 mgal. The far-side topography shows a higher mean elevation, 3–6 km above the mean radius. The basins on the near side, flooded with basalt, are 1–4 km below the mean lunar radius. This lends support to the explanation that the near-side–far-side visual asymmetry for mare lavas is due to the height which the lavas can reach on the basis of density differences. The far-side gravity is less well-known but shows rather broad scale positive features with local negative free-air anomalies over the major ringed basins [18, 19] such as the Mendeleev, Moscoviense, Korolev and Apollo basins which all appear to have strong negative anomalies (about −100 mgal). Basins such as Ingenii have relative gravity lows. The Mendeleev basin, 4 km deep and 300 km in diameter, has a negative anomaly of −116 mgal. Corrections for the topography indicate a positive Bouguer anomaly of +100 mgal. Thus, some isostatic readjustment took place following the basin impact. Mendeleev is Nectarian in age (Table 3.1). This positive gravity anomaly must be due to mantle rebound during basin formation. This seems to be consistent with the Orientale basin evidence. Since there is only a small amount of mare basalt fill in the center of the Orientale ringed basin, most of the positive gravity anomaly must also be due to mantle rebound. The positive anomaly of Grimaldi (+60 mgals) is too large for a 150 km crater, even if filled with lava; other craters of this size show negative anomalies. The paradox is resolved by the recognition that Grimaldi is, in fact, a ringed basin with a diameter of 420 km [20] and a significant part of the positive anomaly is due to mantle rebound. This basin, for which good gravity and topographic data exist, thus provides a key to understanding much of the mascon problem (Fig. 7.3) (see Table 3.1).

A summary of the gravity data indicates that:

(a) Young ray craters have negative Bouguer anomalies, a consequence

both of the mass defect due to excavation and of low density breccia and fall-back within the crater.

(b) Craters less than about 200 km in diameter, filled with lava, also have negative anomalies. Sinus Iridum, the Bay of Rainbows on the coast of the Sea of Rains (Mare Imbrium), has a negative anomaly of −90 mgal.

(c) The older lunar highlands are in isostatic equilbrium and the Imbrian and Pre-Imbrian craters which saturate the highland crustal surface have no Bouguer anomalies indicating probably that there was no mantle rebound.

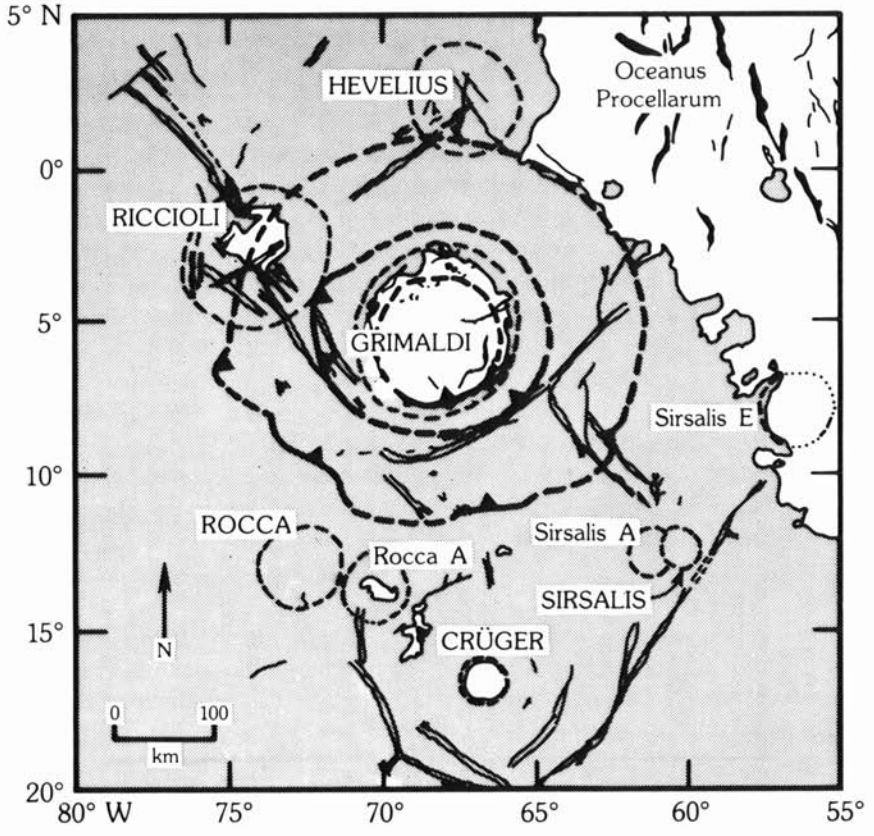

7.3a Tectonic and geologic structure of Grimaldi. Concentric ring structures are shown for Grimaldi as heavy lines, dashed where inferred or extrapolated, with scarps indicated by arrowheads. The innermost ring shown is probably a normal fault resulting from the volcanic load in the central basin. Ridges are shown in the mare-covered central basin of Grimaldi and in Oceanus Procellarum to the northeast. Other structures depicted are rilles [20].

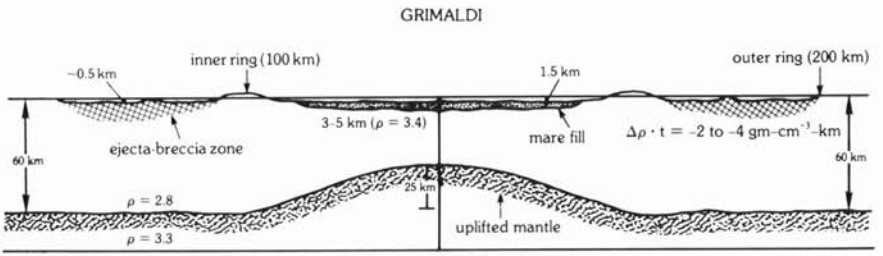

7.3b Schematic cross-section of the Grimaldi basin and inferred subcrustal structure, determined from the gravity data. Horizontal and vertical scales are equal. The ejecta-breccia zone is expressed as a density-thickness product [20].(Courtesy R. J. Phillips.)

(d) The large mountain ranges formed around the young multi-ring basins (e.g., Apennines) are uncompensated and have large positive anomalies, i.e., they are supported by stresses in the rigid lithosphere.

(e) The circular maria on the near side have large positive gravity anomalies. The largest are those of Mare Imbrium and Mare Serenitatis (+220 mgal), with smaller positive anomalies under the circular mare, Crisium, Nectaris, Humorum, Humboltianum, Orientale, Smythii; and under Sinus Aestuum and Grimaldi.

(f) The Marius Hills, widely interpreted as volcanic domes, superimposed on the basaltic maria, show a positive anomaly of +65 mgal, indicating that virtually no late isostatic adjustment has occurred in the mare basalt flooding stage and that these volcanic features are supported by the crust without yielding.

7.4.2 The Mascons

The excess masses represented by the positive gravity anomalies over the circular maria have excited much interest, and yield useful information on the thermal state of the Moon. A key piece of information is the fact that the Apennine ridge is uncompensated [18], showing that the crust was cold enough to support the basin topography at 3.8 aeons. Earlier interpretations indicated that some compensation had occurred, so that the mascons were interpreted to result from later basaltic flooding of the multi-ring basins. However, the thickness of lava fill which would be necessary to account for the mascons is typically 15–20 kilometers. The greatest thickness of mare basalt in multi-ring basins is unlikely to exceed 5 km at most and may be much thinner (Section 6.1.1). Accordingly, although the mare basalt fill does contribute significantly to the excess mass observed, it is inadequate to account for it all.

This rules out ideas that the mascons are due to the accumulation of dense iron-titanium oxides on the bottom of large lava lakes during cooling and crystallization of the lunar basalts. This suggestion encounters the difficulty that there is only limited evidence of near-surface fractionation or sinking of such phases (see Section 6.6.2). Possibly such a mechanism might operate where the lavas are ponded, as in the flooded craters. Such ponding might also occur during the first stages of filling of the impact basins, but there is little evidence of such processes even in such apparently favorable sites as the Taurus-Littrow Valley (Apollo 17) or at the Apollo 15 site (see Section 6.1.3).

The possibility that the mascons are due mainly to the transformation of the lunar basalts to the denser rock, eclogite, at the base of the circular maria is also very unlikely. This transformation, at shallow depths and low temperatures depends critically on the kinetics of the reactions, but the depth of mare basalt fill (< 5 km) is nowhere sufficient to induce this transformation.

One mechanism for the production of the mascons proposes that the ejecta of the ringed basins blankets the surrounding highlands with a low thermal conductivity blanket [21]. This induces melting, and the lavas so generated move laterally to fill the fractured ringed basin. The small amount of fill in Mare Orientale is thought to be due to the excavation of the basin "late in the history of the Moon" [21]. Three objections may be noted: (a) old unflooded basins have been discerned on the far side, (b) the thicker crust on the far side should have caused higher rises in temperature and extensive outpouring of lavas, and (c) the lavas are not thick enough anyway.

The early notion that the mascons are the remnants of the colliding objects (large meteorites, asteroids, or primitive earth satellites), which produced the great mare basins by impact, has been rendered unlikely by our greater understanding of impact mechanics. The projectile does not survive [22].

Slow isostatic mantle response, involving upwelling of the dense lunar mantle, has been shown to be unlikely [23], since many very large Imbrian-age craters (e.g., Neper and Humboldt) should also show positive, not zero, Bouguer anomalies. The case of Grimaldi, whose central crater is the same size as Humboldt, has been noted earlier, but it is now known to represent the central portion of a 430 km diameter basin (Fig. 7.3).

The detailed gravity structures over mascons appear to include a central positive anomaly, flanked by negative anomalies, as are apparently observed at Orientale. Clear examples exist for Grimaldi and Mare Serenitatis, which were directly overflown [20, 24]. The gravity anomalies appear to be modelled best by a rather narrow high density pipe. Such central uplift features are common in complex terrestrial craters (Section 3.5). The negative anomaly surrounding the central positive anomaly may be due to locally thickened crust (S. Pullan, pers. comm., 1981), or a residual from the initial depression filled with breccia. This latter possibility seems more reasonable. Accordingly,

the evidence suggests that the mascons are principally due to rapid mantle uplift (formed immediately as a consequence of the impact and not due to a long-term isostatic response), followed by an additional component due to mare basalt filling (Fig. 7.3).

The loading of the mare basalts on the crustal surface induces the rather mild form of adjustment observed, in the form of wrinkle ridges inside the mare basin due to compressive stress and the formation of curved grabens on the outer edges of the basins due to tensional stresses [24]. Most of the deformation of the lunar crust which is not attributable to impact processes is due to this basaltic loading on the surface.

From these observations, calculations of the thickness of the elastic lithosphere have been made. Some estimates call for a relatively thin (50 ± 25 km) layer at 3.6–3.8 aeons, thickening to about 100 km after 3.6 aeons [25]. Such small thicknesses would impose important constraints on lunar thermal models. Graben type rilles are observed only on mare surfaces older than 3.6 aeons, but wrinkle ridges persist to younger periods [26]. This evidence is often interpreted as the consequence of a global stress system, evolving from a relatively tensional to a compressive system. The very flat floors of the mare lavas in the basins (e.g., Serenitatis) may indicate that this very mild tectonic regime is local rather than of moon-wide extent. Theoretical calculations employing sophisticated models indicate that the low values of 100 km or so for the thickness of the elastic lithosphere may be serious underestimates and that the stress-bearing layer may be much thicker [27]. Accordingly, the use of these small lunar surface tectonic features to deduce lunar thermal history does not provide tight constraints [27]. A final comment on mascons relates to the possibility of bringing mantle material within reach of sampling. Successive impacts may bring deep material near to the surface. Possibly the observation that the central peak of Copernicus (Chapter 3) may be composed of olivine can be explained by such processes. Perhaps also some of the Mg-suite rocks owe their origin to such uplifts.

7.4.3 Mars

Martian gravity is dominated by the Tharsis plateau [2, 16] (Fig. 7.4a). Most of the other Martian topography appears to be in a state of isostatic compensation. A basic geophysical question is how the excess mass represented by the Tharsis Plateau is supported. The age of the plateau from crater counting is possibly 3 aeons. If this load is supported statically, a compensation depth (i.e., thickness of the lithosphere) is about 300 km. An alternative suggestion is that the plateau is supported dynamically, possibly by convection. The Tharsis Plateau has the most anomalous gravity features of all the terrestrial planets.

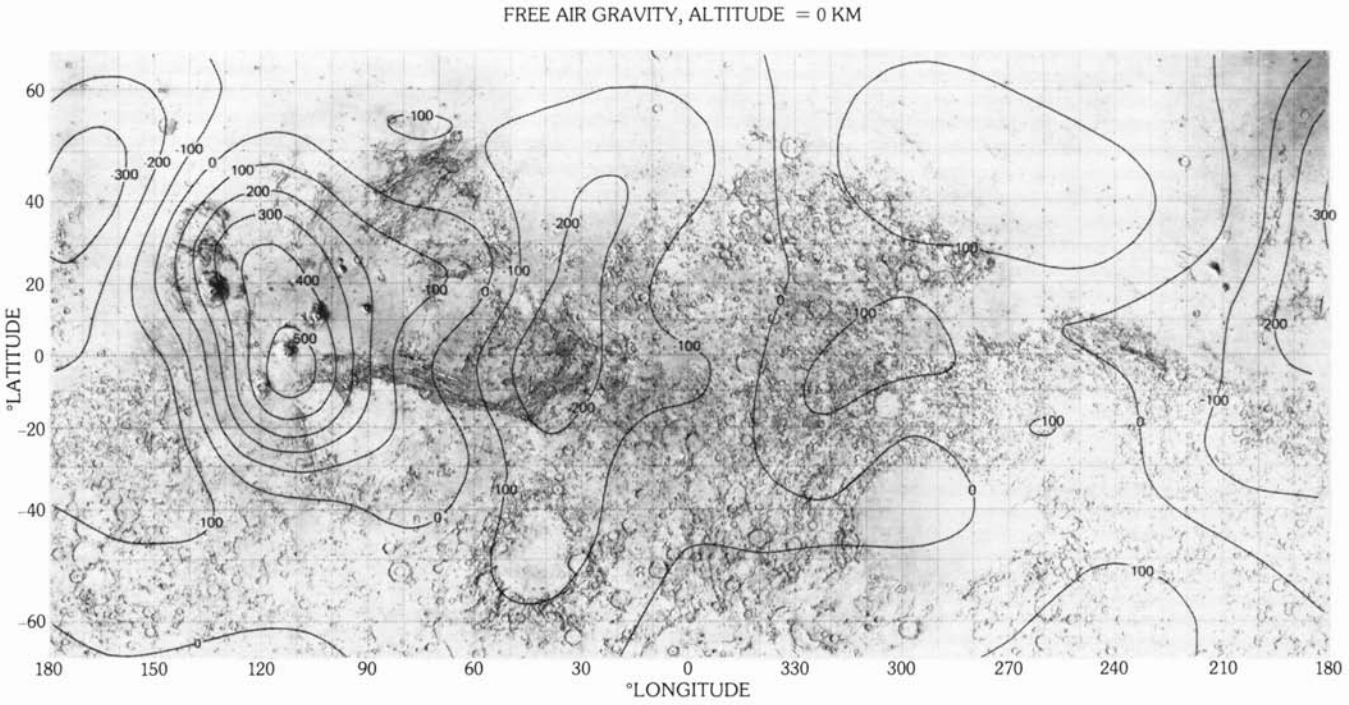

7.4a Low-order spherical harmonic free-air gravity field for Mars showing the dominance of the Tharsis anomaly. Contour values in mgals. (Courtesy R. J. Phillips.)

The large volcano, Olympus Mons, may be uncompensated [28], but this is uncertain. The other large shield volcanoes may be locally compensated [29]. Olympus Mons should exert tensional stresses of the order of one kilobar, for a lithospheric thickness of 200 km. Possibly there is a local thick lithosphere under Olympus Mons [30, 31] and possibly there is some subsidence, the evidence for which is concealed beneath the younger flows which drape the scarp around the foot of the mountain. Clearly many more data for Mars are required, particularly on the elevation of the Tharsis region. Recent radar data support the concept of a trough-like subsidence around Olympus Mons (P. Mouginis-Mark, pers. comm., 1981) and indicate that the Tharsis Plateau relief is some 2–5 km lower than previously thought.

7.4.4 Venus

The Venus gravity field shows a strong positive correlation with topography (Fig. 7.4b) in contrast to the Earth. A very thick lithosphere (i.e., a low temperature gradient) would be required to support these loads statically if the surface is ancient. If the circular features on the plains are impact craters, then the mean surface age is of the order of 2 billion years [31]. If the radioactive element concentrations in Venus approximate those of the Earth, then it appears unlikely that such topography can be supported against creep for such periods. Accordingly, dynamic support of the topography, in particular the high standing masses of Ishtar Terra and Aphrodite Terra, is called for.

7.5 Seismology

7.5.1 The Lunar Record

The lunar seismic signals have very low attenuation [32] and a large degree of wave scattering [33–34]. The scattering occurs mostly in the upper few hundred meters, which is highly heterogeneous, but significant scattering extends to depths of 10–20 km and is due to the extensively fractured nature of the crust. The lunar crust appears to be heterogeneous at all size ranges up to several kilometers. The absence of water and volatile constituents allows the seismic signals to propagate with little or no attenuation [34, 35].

The observed moonquakes are all less than about three on the Richter scale and so compare with only the smallest of terrestrial earthquakes [33]. The number recorded per year is less than 3000. The total energy release per year by moonquakes is 2×10^{13} ergs, compared to 10^{24}–10^{25} ergs by earthquakes. The total lunar energy release is less than that of about 500 g of TNT. About 10% of them are repetitive, and many sets of nearly identical wave trains have been observed [35]. This important observation means that the

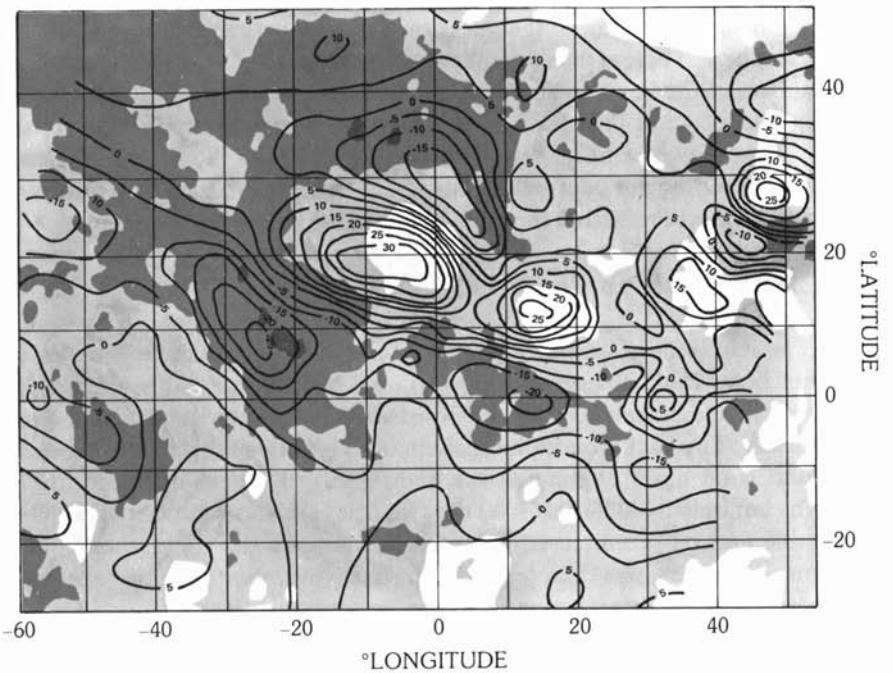

7.4b Line-of-sight gravity measurements in mgals for the central portion of Venus (cf. Fig. 2.25) where the line-of-sight direction for the Pioneer Venus spacecraft was essentially vertical to the surface. Gravity data are superimposed on topography shaded at about 1 km intervals. Lighter shading indicates higher elevation. Note the very clear correlation between gravity and topography for Venus. (Adapted from [16].)

locations and mechanisms are fixed. In addition, it is noted that the deep-focus moonquake activity occurs usually at a fixed phase of the lunar tidal cycle.

Thirty-seven active moonquakes foci have been located. These lie in two belts along great circles. The eastern belt intercepts the western one at about 80° in a T-junction. The western belt lies along one of the rays of Tycho, which also follows a great circle. Most occur at depths of around 1000 km, centered on the lithosphere-asthenosphere boundary. A few occur at depths of less than about 100 km. These so-called high frequency teleseismic events are probably associated with thermal and tidal stresses acting on the deep fractures surrounding the multi-ring basins [36]. As such, they are the only present form of lunar tectonism. These events are the most energetic of the moonquakes.

The Moon is thus almost inert compared with the Earth. Tidal energy, not heat energy as in the Earth, is the driving force for most of the weak lunar

seismic events. The thick lunar lithosphere is almost stable, and moonquake activity is concentrated at the transition region between lithosphere and asthenosphere. There is thus a great contrast between the active, unstable thin lithosphere of the Earth, which is driven by an active thermal engine and the stable lithosphere of the Moon, which is an order of magnitude thicker.

The paucity of shallow seismic activity means that the Moon is neither rapidly expanding nor contracting at present. No seismic activity is observed along the lunar rilles within the limits of detection of the lunar seismometers.

7.5.2 The Martian Record

The seismometer on the Viking Lander 2 in Utopia Planitia is mounted on the lander itself (for weight reasons), and so is considerably affected by wind noise. Nevertheless, it has demonstrated that Mars is extremely quiet seismically. The background microseism level is below the detection threshold, and wind noise dominated the data. The instrument operated for 19 months but only 2100 hours (16%) of low noise level data was obtained. One probable natural seismic event of intensity three on the Richter scale, at a distance of 110 km, was detected on SOL 80 in November 1976, three months after the landing. This is probably a local seismic event or meteorite impact, although a wind noise origin cannot be completely excluded [37, 38].

7.6 Internal Structures

7.6.1 The Moon

The structure of the lunar regolith, as revealed by seismic data, has been discussed in Section 4.3. The lunar crust (Section 5.1), which is less dense and chemically distinct from the interior, varies from an average thickness of 64 km on the near side to 86 km on the far side, with an average thickness of 74 km. Recent refinements of the seismic data may indicate a near-side crustal thickness of 50 km (Y. Nakamura, pers. comm., 1981). This would indicate an overall thickness of about 60 km, 10% of lunar volume. The mare basalts, although prominent visually, constitute less than 1% of the crustal volume (0.1% of lunar volume). A 20-km discontinuity within the crust does not reflect the base of the mare basalts, but rather the depth of fracturing or of closure of cracks produced by the large collisions, thus representing the change from fractured to competent rock (Section 5.3). The subsurface structure in the mare basins has been revealed by the Lunar Sounder experiment [39] (see Section 6.1.1).

For depths down to 150 km, information comes mainly from data recorded on the seismic network from the Saturn IV B booster and LM ascent

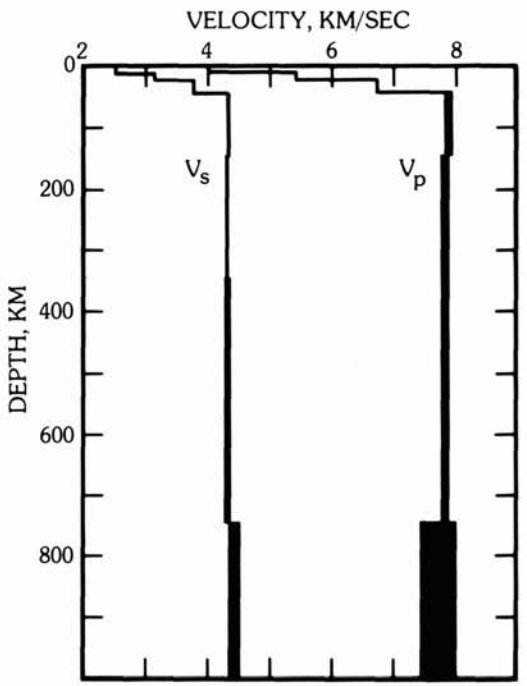

7.5 The crustal and mantle velocity structure of the Moon. The crustal model is derived from artificial impact data, and the mantle is mainly from natural event data. Solid regions represent the uncertainty of the estimated velocities [36]. The most recent interpretation of the seismic data does not allow resolution of the small changes in V_p and V_S in the mantle. The lunar crust may be about 10 km thinner than previous estimates (Y. Nakamura, pers. comm., 1981).

stage impacts. Source to station distances range from 8.7 to 1750 km. Seismic signals from distant meteorite impacts and from moonquakes provide data for regions below 150 km [33–36].

The lithosphere extends to about 1000 km depth [40] (Fig. 7.5). The average P-wave velocity (V_p) is 7.7 km/sec and the average S-wave velocity (V_S) 4.45 km/sec, with negative velocity gradients. There is some inconclusive evidence for lateral heterogeneity [41].

On the basis of the lunar seismic data, Goins and coworkers [40] proposed a model for the structure of the lunar interior. Their preferred model calls for a minor discontinuity, possibly located at a depth of 400–480 km, with a change to lower seismic wave velocities (V_p = 7.6 km/sec; V_S = 4.2 km/sec) down to depths of about 1000 km. Whether this discontinuity really exists, or whether it is located at a different depth, does not appear to be resolvable from the present seismic data. The model is based mainly on the differences in S-wave velocities and the P-wave data do not show such a marked change. If there is a real change in the V_S values above and below 400–480 km, then many models of the lunar interior structure would satisfy the data. The geochemical and petrological consequences of such a discontinuity, if firmly established, are considerable. It could mark the base of the

outer melting zone, and thus might represent a fundamental break between upper fractionated material and lower primitive compositions. Since the lower regions would contain their original complement of radioactive elements, some partial melting might be expected, as well as the presence of denser phases such as garnet. Since the preferred model of Goins and coworkers [40] of a transition zone between 400 and 480 km depth does not appear to be demanded by the seismic data (see discussion by Cleary [42]), it is not adopted here as a constraint. It is clear that the problem will not be resolved like so many others, until seismometers are once again operating on the lunar surface. The geochemical evidence can be interpreted to indicate that melting of the Moon was deeper than 400–480 km (Sections 5.11 and 6.5). If a core exists, then whole-moon differentiation probably was involved and the lunar mantle structure might be complex in detail, as is suggested by the variety of lunar basalts which have been collected. If solid state convection existed until 3 aeons, then the structures revealed by seismic studies might represent only the final condition, and provide no evidence on the earlier structures, as is assumed here.

The mantle P-wave and S-wave velocities continue to about 1100 km without much change [40]. Deep within this zone (800–1000 km depth) occur most of the moonquakes. Below 1100 km, the structure becomes less certain. P and S waves become attenuated ($V_S = 2.5$ km/sec), consistent with the presence of some melt. This marks a major discontinuity, with a very sharp decrease in the S-wave velocities. The evidence came from a single event: impact of a large meteorite (weighing about 1 ton) on the far side of the Moon in July, 1972. P waves were transmitted, with slightly lower velocities through the Moon, but S (shear) waves, which are not transmitted through liquids, were missing, indicating a central zone of a few hundred kilometers radius, below a depth of about 1000 km, with differing properties. Either the shear waves did not propagate at all or were so highly attenuated as not to be recorded.

7.6.2 A Lunar Core?

The possible existence of a lunar core has been much debated. Conclusive evidence for its existence has not been obtained from seismic, magnetic field, or moment-of-inertia data. The value for coefficient of moment of inertia (0.391 ± 0.002) (Table 7.1) is low enough to require a density increase in the deep interior, in addition to a low density crust. It would be satisfied by a core, the presence of dense phases such as garnet, or a more primitive iron-rich silicate interior. A recent reassessment of the deep lunar electrical conductivity profile [43] places an upper limit of 360 km on a metallic core, but the error limits are large. An assessment of the magnetic data from the Apollo subsatellite magnetometer strongly suggests the presence of a central conducting

Table 7.1 Radii, densities and moments of inertia for some solar system planets and satellites.

	R (km)	±	Density g/cm^3	±	I/MR^2	±
Mercury	2439	2.0	5.435	0.008	—	—
Venus	6051	0.1	5.245	0.005	—	—
Earth	6731	0.005	5.514	0.005	0.3315	0
Moon	1738	0.1	3.344	0.003	0.391	0.002
Mars	3390	1.0	3.934	0.004	0.365	0.005
Phobos	$27 \times 21 \times 19$	—	1.9	0.6	—	—
Deimos	$15 \times 12 \times 11$	—	—	—	—	—
Io	1816	5	3.55	0.03	—	—
Europa	1536	10	2.99	0.06	—	—
Ganymede	2638	10	1.93	0.02	—	—
Callisto	2410	10	1.83	0.02	—	—
Mimas	195	5	1.2	0.1	—	—
Enceladus	250	10	1.1	0.6	—	—
Tethys	525	10	1.0	0.1	—	—
Dione	560	10	1.4	0.1	—	—
Rhea	765	10	1.3	0.1	—	—
Titan	2572	26	1.9	0.06	—	—
Hyperion	145	20	—	—	—	—
Iapetus	720	20	1.2	0.5	—	—
Vesta	269	—	2.9	0.5	—	—

region of 400–500 km radius [44]. Limits on core sizes vary somewhat from different workers, with estimates of up to 300–400 km radius for a metallic core and 500–600 km for one of FeS [45]. In addition, zoned cores, comprising an inner solid iron core surrounded by a molten FeS core, have been proposed [46]. (For further discussions of lunar cores, see [47, 48].)

In summary, the geophysical evidence for the existence of a core has become slightly stronger, but it is still not demanded by the data. Only further lunar missions will ultimately solve this problem. The view is adopted here that the presence of a core is consistent with the overall evaluation of the geochemical data and is not inconsistent with the geophysical evidence. Several possible models of the lunar interior are shown in Fig. 7.6.

7.6.3 Mars, Venus and Mercury

The internal structures of these three planets are heavily model dependent. An extended discussion is given in Chapter 4 of *Basaltic Volcanism on the Terrestrial Planets* (see Table 8.5 for mantle and core compositions of these planets) and only an outline indicating the various limits is given here.

It is generally agreed that Mercury must possess a metallic core. Estimates vary from 65 to 68 wt.% of the planet, with an overlying silicate mantle.

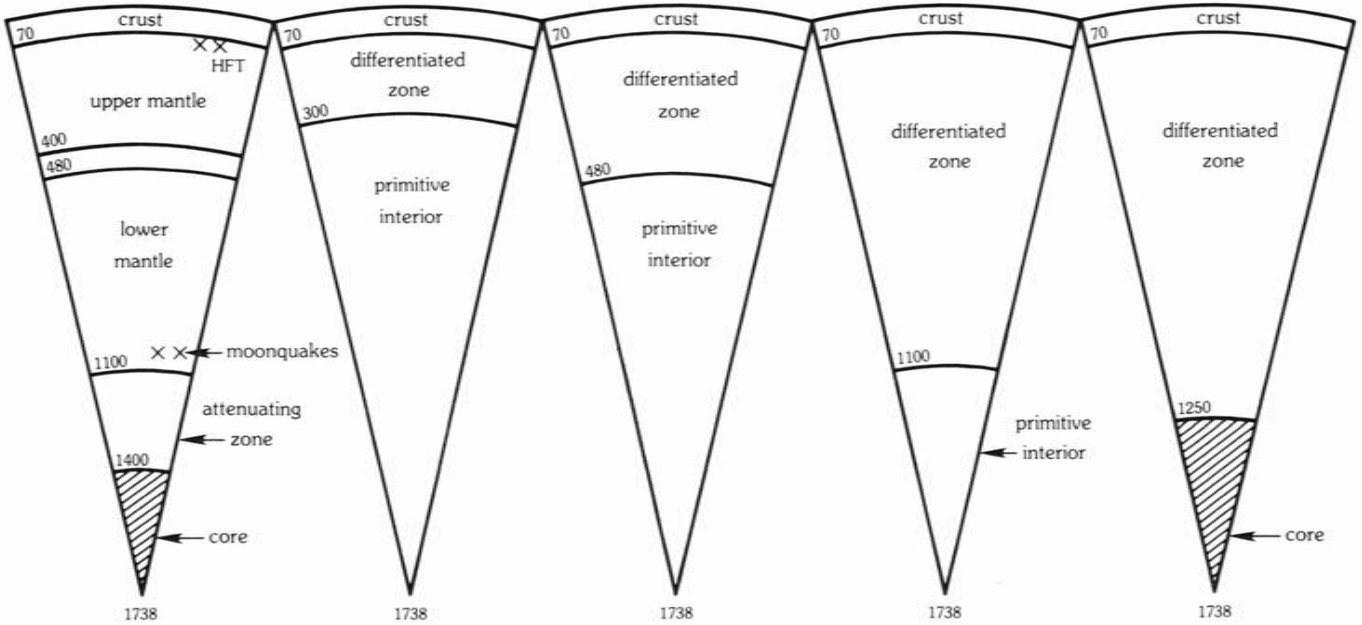

7.6 Five possible internal structural models for the Moon. The model on the left shows an interpretation of the seismic data due to Goins et al. [40]. The division into upper and lower mantle is non-unique [42]. The second model shows a lunar structure due to a shallow depth of melting, leaving a primitive undifferentiated interior [25]. In the third model the depth of initial melting is 480 km, consistent with the Goins et al. [40] interpretation, leaving a primitive undifferentiated interior. The fourth model illustrates an initial depth of melting to the base of the attenuating zone. In the fifth model on the right, the entire Moon has differentiated. A small core has formed and the mantle is comprised of cumulates (olivine, orthopyroxene and clinopyroxene), overlain by the feldspathic crust. This model is preferred as being most consistent with the geochemical data.

The low density and high value for the coefficient of the moment of inertia of Mars compared to the Earth indicate a differing bulk composition (Chapter 8) and internal structure. The geophysical constraints limit mantle densities to between 3.43 and 3.54 g/cm^3. Using reasonable estimates for bulk compositions, core densities are constrained between 5.6 and 7.9 g/cm^3, and the weight percent of cores to about 20%.

The bulk density of Venus is about 2% lower than if it had the same bulk composition as the Earth. Core densities in various models range from 6.7 to 7.9 g/cm^3 and the wt.% of the core from 28 to 32%. Phase transitions in the mantle, as on Earth, are predicted at depths of 450–750 km. Densities and radii of the Galilean and Saturnian satellites are given in Table 7.1.

7.7 Heat Flow and Internal Temperatures

7.7.1 Heat-Flow Data

The lunar heat-flow measurements were less fortunate than any other aspect of the Apollo missions. A heat-flow probe was on board the aborted Apollo 13 mission. It was not carried on Apollo 14. The first measurements were made at the Hadley Apennines site (Apollo 15) on the mare surface. The long awaited result from the highlands site at Descartes was lost due to a broken cable. Some variation with depth was encountered in one probe at the Apollo 17 site, but the heat flow at the bottom of the holes (1.3 and 2.3 m in depth) was similar to that at the Apollo 15 site.

The revised heat-flow values at the Apollo 15 Hadley Rille and Apollo 17 Taurus-Littrow sites are 2.1 and 1.6 μw/cm^2 [49, 50].

7.7.2 Electrical Conductivity

Lunar electrical conductivity measurements can be made by recording the electromagnetic response of the Moon to the magnetic field variations in the solar wind. It is also possible to invert the electrical conductivity profiles to temperatures at depths within the Moon. The basic information is obtained from the surface magnetometers and orbiting spacecraft. Conversion to a temperature profile is beset with difficulty, since the composition of the interior must be inferred from other evidence.

The first results showed a conductivity "spike" at a depth of 240 km [51], but other work showed that a two-layer model with a boundary at 160 km depth was consistent with the same data, and the spike is not a unique or necessary feature [52]. The early temperature profiles [51] are much too low, due to the fact that olivine containing ferric iron was used for calibration purposes.

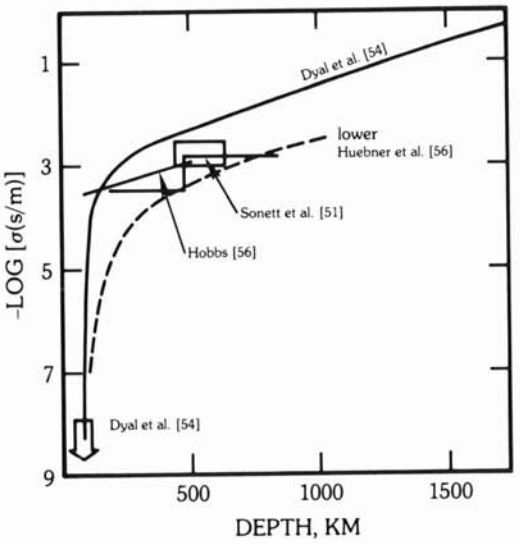

7.7a The variation of lunar electrical conductivity with depth based on electromagnetic sounding [51, 54, 56].

Later values for the conductivity of the lunar interior were provided by Dyal [53, 54], Vanyan [55], Huebner et al. [56], Herbert et al. and Hood et al. [57]. The latest estimate of conductivity with depth is given in Fig. 7.7a, based on these various estimates.

7.7.3 The Lunar Temperature Profile

Various methods are available to estimate the temperature in the lunar interior. These include the following:

(a) Calculations from the heat-flow data, assuming a steady-state thermal model for the upper mantle [50].
(b) Thermal model calculations [58].
(c) Utilizing the stress state calculated from the lunar gravity and topography data [59, 60].
(d) Obtaining electrical conductivity profiles from the magnetic data, and using these to obtain temperatures [54, 56, 61].

Various constraints are available from the mascon data (Section 7.4.2) which imply significant lithospheric strength at 3.8 aeons. Most of the lunar gravity anomalies are near surface. If the internal temperatures are above a certain value, the presently observed topography and gravity anomalies should have vanished in the past 3.8 aeons. Pullan and Lambeck [12] conclude that the "temperature at 300–400 km depth must be 200–300° C less than that proposed by Duba et al." [60]. It should be recalled that all models of load support are dependent on the laboratory data for strain rates in dry

olivine. They also conclude that the Moon has undergone little thermal evolution in the past 3 aeons (e.g., [58]), in contrast with other thermal evolution models, which had thin (100 km) lithosphere at 4 aeons. The thickness of the lithosphere at the time of mascon formation was probably about 400 km in order to support the stress differences of 70 bars [61]. It should be recalled that the mare basalts comprise only 0.1% of the volume of the Moon and do not require that the entire interior, or even more than about 1%, approach melting temperatures. Partial melting induced by localized concentrations of the heat-producing elements is adequate to account for the volcanic activity. The large surface area/volume ratio of the Moon indicates that much of the Moon's internal heat has been lost, which would argue for a near steady-state heat flow, and thus for uranium values of up to 45 ppb (Section 8.6). The value of uranium adopted here (Table 8.1) for the bulk moon is 33 ppb, which is a highly conservative estimate. From the various isotopic constraints, it is clear that substantial proportions of the lunar heat producing elements were concentrated near the surface at 4.4 aeons, while the remainder were mainly concentrated in the source regions of the mare basalts. If the Moon was totally differentiated, and possesses a small core, then little K, U and Th is left in the very deep interior. This would also be in accord with low present-day internal temperatures. Thus, Lambeck and Pullan [59] argue for temperatures as low as 800° C at depths of 300 km, compared with values from 900 to 1100° C estimated from the electrical conductivity models. These low temperatures are in accord with the observed low state of lunar activity

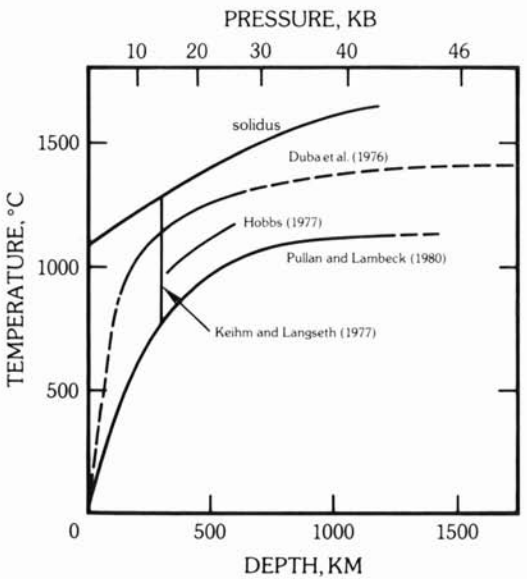

7.7b Lunar temperature profiles with depth, calculated from the conductivity data [56, 60] and by considering the internal stress state [12]. The limits suggested by Keihm and Langseth [50] from the heat flow data are shown.

for the past 3 aeons, but new data will be required to resolve this question. The ranges in internal lunar temperatures from these constraints are given in Fig. 7.7b.

7.8 Magnetic Properties

7.8.1 Lunar Magnetism

The present global lunar magnetic field, as measured by the early Explorer satellites, is vanishingly small, but among the surprises contained in the returned Apollo 11 samples was evidence of a stable natural remanent magnetism (NRM) in the rocks, suggestive of an ancient field, now vanished [62–65].

The surface magnetometer experiment on Apollo 12 measured a remanent magnetic field of 38 gamma [63]. Only 6 gamma was recorded at the Hadley-Apennine site, again on mare basalt. The highland sites, in contrast to the maria, showed evidence of higher fields. At the Apollo 14 Fra Mauro location, values of 43 and 103 gamma were obtained at two separate locations, and 121 to 313 gamma at the Apollo 16 Descartes site. The last value was measured at North Ray crater rim and is the highest recorded on the Moon. These relatively strong surface fields in the highlands affect both the implantation of outgassed ions and the accretion of solar wind particles [64, 65].

A third set of observations of lunar magnetism were made by orbiting magnetometers and charged-particle detectors on the "subsatellites" launched from the Apollo 15 and 16 command modules [66]. The Apollo 15 system operated for 6 months. Local magnetic anomalies on the lunar surface were observed for the first time. Most of the measurements of lunar fields were made during the five days around full-moon when the Moon is in the geomagnetic tail of the Earth; this provides a relatively low noise environment for mapping the lunar surface magnetic fields.

7.8.2 Remanent Magnetism

Magnetic data provide many potential constraints on planetary evolution and history. For example, the presence or absence of a conducting core may be inferred. Hence, the report of a stable remanent magnetism (NRM) in the Apollo samples excited much interest.

Many components of magnetism are present in the lunar rocks. One is a "soft" component, most of which is acquired through exposure to magnetic fields during sample return from the Moon. This was demonstrated by returning a demagnetized Apollo 12 basalt (12002, with a very low "hard" compo-

nent) to the Moon during the Apollo 16 mission. The sample reacquired its "soft" component, indicating that this was at least in part an artifact of the trip [67].

Metallic iron has been identified as the dominant magnetic material in lunar samples [68]. Most Curie temperatures are around 750–770° C, close to that for pure iron. This is in contrast to the Earth, where the major magnetic materials are the Fe oxides within the system $FeO\text{-}TiO_2\text{-}Fe_2O_3$. Most of the lunar iron is very fine and is attributed, because of its low nickel content, to autoreduction in glass spherules formed during impact (see Section 4.5.1). No magnetic effects attributable to troilite have been noted, indicating that troilite is stoichiometric FeS.

The identification of the magnetic phase in lunar fines as metallic iron appears to have been confirmed by electron spin resonance (ESR) techniques [69, 70] (see Section 4.5.1), refuting earlier suggestions that hematite, magnetite, or ferric oxides with magnetite-type lattices were present. The absence of Fe^{3+} in ilmenite and ulvöspinel is indicated by their lack of ferromagnetic properties. Magnetite appears to be absent, except for one possible occurrence in the Apollo 17 orange soil. The magnetic data accordingly support the petrological interpretations of extreme reducing conditions (Section 6.2.2).

A hard component of magnetization in the samples is of lunar origin. The basalts have stable remnant magnetizations with intensities of $1\text{–}2 \times 10^{-6}$ emu/g. Some breccias have much larger intensities, on the order of 1×10^{-4} emu/g, accounting for the observed surface anomalies. This increase is correlated with the content of total metallic iron in the breccias and to changes in grain size. The samples collected on the present surface had random magnetic orientation. Accordingly, they were magnetized before being excavated by meteorite impact and thrown onto the lunar surface.

The magnetic properties measured in the highlands breccias have the following characteristics.

(a) The unwelded breccias resemble the soils. Most of the iron particles are less than 150 Å in diameter, and they have low thermoremanance. The magnetic component in the soils is in the finest-grain size [71].

(b) The intermediate grades of breccias are dominated by single domain iron (150–300 Å grain size) and possess a strong thermoremanance.

(c) The highly crystallized breccias contain multi-domain iron (300 Å grain size) and do not carry a strong remanent magnetism. In this they resemble the igneous rocks from the maria, except that they tend to be magnetically inhomogeneous and contain a high content of metallic iron.

Using these criteria, the anorthositic gabbro 68415 for example is not igneous but a strongly recrystallized breccia, a view in accord with the chemical and age characteristics of the sample. Experiments have shown that annealing at temperatures below 900° C produces the fine-grained iron (100

Å) typical of soils and soil breccias [71]. At higher temperatures, coarser grains up to micron size are produced by autoreduction processes.

This correlation of iron grain size and content with metamorphic grade indicates that the breccias have both higher metallic iron contents than the mare basalts and higher thermoremanant magnetism. These effects occur in recrystallized samples that have been heated in impact events indicating that such processes cause enhancement of the sample magnetization.

7.8.3 Lunar Magnetic Field Paleointensities

Considerable efforts have been made to determine the paleointensity of the vanished field. A basic problem in making lunar paleomagnetic measurements is to avoid inducing chemical changes in the samples during heating experiments. The lunar magnetic memory is carried by metallic iron, much of it in a size range of a few hundred angstroms. Many of the problems encountered in the early stages of magnetic studies on the lunar samples were probably due to alteration of this fine-grained iron in the strongly oxidizing and moist terrestrial environment. Recent sample preparation techniques have been devised so that oxidation or reduction can be avoided during thermal treatment [72].

A review of magnetic paleointensity methods [73] which compares four methods of determining paleointensity concludes that only the Thellier method applied using the new sample preparation method [73] appears to provide reliable estimates. Of the five published results considered to be reliable (Table 7.2), none show any clear evidence of a strong correlation with

Table 7.2 Reliable estimates of lunar magnetic paleointensity.

Sample	Paleointensity (Oersteds)	Method	Age (aeons)	Reference
70019	0.025	Thellier	0.003	1
15498	0.021–0.05	Thellier	<3.3	2
70215	0.02–0.075	Thellier	3.84	3
	0.06	ARM†		3
62235	1.2	Thellier	3.9	4
	1.4	ARM†		3
60255	0.005	Thellier	3.9	5

†ARM = Anhysteretic remanent magnetization.

1. Sugiura, N., et al. (1979) *PLC 10*: 2189.
2. Gose, W. A., et al. (1973) *Moon* 5: 196.
3. Stephenson, A., et al. (1974) *PLC 5*: 2859.
4. Collinson, D. W., et al (1973) *PLC 4:* 2977.
5. Sugiura, N. and Strangway, D. W. (1980) *PLC 11*: 1801. (Table adapted from this source.)

time for an ancient lunar magnetic field. More data are clearly required (Fig. 7.8).

A field intensity of 2500 nT or gamma (= 0.025 Oersteds) was measured for a very young impact glass lining a 3-m crater at the Apollo 17 landing site [74]. The exposure age of the glass is less than 3 million years [75]. The source of the magnetizing field can be neither the extinct dynamo, nor an internal primordial memory, since both sources are no longer extant. Two explanations are possible: (a) there is today a local permanent field of 2500 gamma at the Apollo 17 site, which magnetized the impact glass as it cooled through its Curie point. Unfortunately, no measurements of the magnetic field were carried out [76]. (b) Plasma processes in the impact which produced the glass may have enhanced a much weaker local field [77], but probably a larger impact is needed for this mechanism to operate. Some combination of shock and rapid thermal quenching might account for the observed magnetization. The association of strong magnetic anomalies with features such as the Reiner Gamma swirl [79, 80] which are in some way connected with impact events [81] lends some credence to this view. The surprising result is that fields of the order of a few tenths of an Oersted were present or enhanced during the formation of some of the soil breccias, which often carry multiple weak components of magnetization. These remagnetizations have widely scattered directions, suggesting that multiple events such as major impacts are responsible for their features.

7.8.4 Crustal Magnetic Anomalies

Observations both by surface-based magnetometers and by those aboard the subsatellites revealed the moon-wide nature of crustal magnetic anomalies. Some correlations with surface geological features have been observed. Many of the anomalies appear to be correlated with ejecta blankets from the

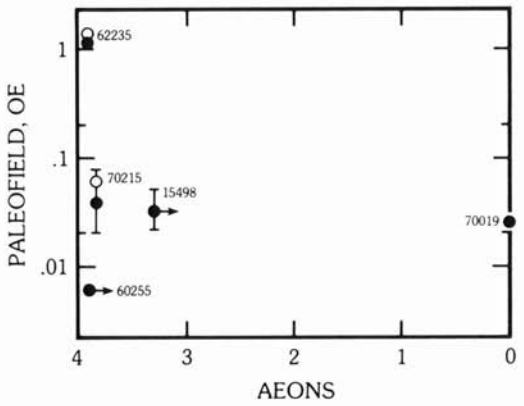

7.8 Ancient lunar magnetic field intensities, plotted as a function of time. Sample 70019 is a young impact glass formed about 3 m.y. ago [73, 74].

multi-ring basins [76]. The youngest identifiable area with an anomaly is the swirl-like feature Reiner Gamma, dated stratigraphically at 100 million years [81] but it may be as old as 2900 million years [79].

A similar correlation is reported with parts of the Fra Mauro Formation, which appears to be magnetized very heterogeneously, in contrast to the rather uniform magnetization observed at Reiner Gamma. Other correlations of surface magnetic anomalies associated with swirls have been reported [80]. Whether these are associated with impact (the swirls show a tendency to be antipodal to large multi-ring basins) remains conjectural [81] (see Section 3.15). This surface field variability seems consistent with impact-induced enhancement in a pre-existing weak ambient field. Temperatures above the Curie temperature of iron (750° C) must have been reached. A possible scenario is that autoreduction of iron oxides takes place during impact glass formation. The pre-existing field is enhanced momentarily during the impact event. Cooling of the glass and the tiny iron spherules occurs rapidly enough for this field to be recorded.

7.8.5 Origin of the Lunar Magnetic Field

A strong moon-wide field, with intensities of up to 1 Oersted, appears to have been in existence at about 4 aeons, but is no longer present.

A wide variety of hypotheses have been offered to account for this vanished phenomena. Just as it is difficult to infer the form of the Cheshire Cat from its smile, so it is equally difficult to produce a credible image of the nature of the magnetic field. The only consensus appears to be that the lunar rocks became magnetized both by weak (< 20 kbar) shock processes and as they cooled through the Curie temperature for metallic iron (780° C) in the presence of a magnetic field.

The resolution of the magnetic debate is of interest to all lunar scientists. If a core is shown to be present, it has considerable geochemical as well as geophysical consequences, implying probable total melting of the Moon, and providing a possible sink for the siderophile elements.

The origins proposed for the lunar magnetic field encompass a large number of processes [82] that fall within the following categories: (a) random fields due to localized near-surface origin; (b) external uniform fields; (c) internal dipole field. Some comments on various proposed models follow.

Impact-generated fields.

Many suggestions have been made that the magnetic effects are in some manner connected with impact processes. A review of these has been given by Fuller [64]. The large scale and number of impact events lends some credence to these theories, but experimental evidence for strong fields in impacts is lacking [83].

Raisin model.

In this variation, small pockets of molten iron collect during differentiation, and act as small dynamos [84]. A variation of this would be the interaction of molten magma with the solar wind [85]. Again, one faces the problem of maintaining such fields over long periods. They do not explain the magnetization of the breccias. Most of the mare basalts were extruded as thin flows so that accumulation of molten iron pockets or the formation of deep lava lakes (except very locally) is petrologically very unlikely.

Earth's field.

The present magnetic field of the Earth at the Roché limit (2.4 earth radii) is 4000 gamma. If the Moon had been just outside the Roché limit, the appropriate field would be available. A major difficulty lies in keeping the Moon at such a close distance for more than 1 aeon. Very large tidal effects would have been present during the extrusion of the mare basalts. There seems to be no evidence of this or other features indicating such a close approach.

Enhanced solar wind field.

It is possible that the solar wind field, at present about 10 gamma, was 100 times more intense [86]. While such strong fields may exist in early stages of stellar evolution, it would be necessary to maintain this high value for more than 1 aeon, with a steady component along the axis of rotation of the Moon. This seems unlikely. Such activity is unlikely to occur from a main sequence star and persist for this period of time, when all geological evidence points toward a sun similar to the present-day one at least during the period 3.5–3.0 aeons (Chapter 9). A major difficulty with this and with all external field theories is that it is very difficult to provide a steady field in a single direction over expected cooling times.

Permanent magnet model.

For more than 300 years, the only explanation of the Earth's magnetic field was that it was due to permanent magnetism. This theory eventually failed to account for rapidly varying terrestrial field changes and many other features, and was discarded and effectively forgotten until recently resurrected for the Moon [87]. The model depends on accretion of the Moon from a sphere of dust and gas in which the solids settled. As contraction occurs, the temperature rises, and eventually the outer solid layers melt. High magnetic fields will occur in the contracting gas sphere, perhaps due to an enhanced solar field; the remnant magnetization of some meteorites may be evidence of this. A variation of this hypothesis supposes that the Moon became magnetized by an early field of perhaps 20 gauss, either through close approach to the Earth or because of enhanced solar wind reaction. The cold inner portion

of the Moon (below 780° C) is magnetized while the exterior is hot. This would most likely be at 4.6 aeons or shortly thereafter. Subsequently, the crust cools and becomes magnetized. Next the interior heats above 780° C and erases the internal field, so that no field is now observed [88].

This is an ingenious suggestion, although it is linked to a specific model of lunar formation, not easily reconciled with the evidence in favor of the planetesimal hypothesis, discussed in Chapter 9.

Fluid core model.

This model deserves close scrutiny since the origin of the Earth's magnetic field is due to the dynamo action in the Ni-Fe conducting core [63–65]. The geophysical data (Section 7.6.2) permit this process, but restrict core radii to less than 400–600 km. Whether such a small core (1–4% of lunar volume) could produce a dynamo has also been debated.

The imprint of a magnetic dipole field on the lunar crust as it cooled through the Curie point would imply the existence of a very early field, but such a distribution is not seen [89–90]. Even if only a weak field were present, it could be pumped up locally by impact-induced magnetism, which can operate provided an ambient field is present [63–65]. Such a mechanism could account for the random and highly variable fields observed at present on the surface (Section 7.8.1). In retrospect, the study of lunar magnetism has provided much stimulus to scientific thinking, as is attested by the volume of literature on the topic. Great contrasts exist with the terrestrial magnetic signatures, carried by oxide minerals in contrast to the very fine-grained iron in the lunar samples. The association of the magnetic anomalies with breccia sheets on the Moon is instructive. Fine-grained iron formed by reduction in impact glasses is preserving a record of perhaps very transient fields. The random orientations observed on kilometer scales are presumably due both to the ejection process and to subsequent smaller cratering events.

7.8.6 Planetary Magnetic Fields

The information obtained from observations of magnetic fields on other planets can help shed light on the problem of the origin of the lunar field.

Mercury has a small but measurable field, with a field strength about one percent of that of the Earth [91], but strong enough to deflect the solar wind and to form a detached bow shock wave. The magnetic dipole moment is 6×10^{-4} that of the Earth. As is the case for the Moon, the origin of this field is uncertain. Active dynamos and remanent fields have both been suggested. The field is clearly of internal origin. It is too large to be caused by a present-day induction process. If it is due to a permanently magnetized crust resulting from an ancient external field, then the crust must have cooled through the Curie point in the presence of this field. However, the lengthy time taken for this cooling rules out unidirectional external fields. If a former

Table 7.3 Planetary magnetic dipole moments.†

Planet	Core Radius, km	Spin Rate, day^{-1}	Dipole Moment G/cm^3
Mercury	~1800	0.017	$\sim 4 \times 10^{22}$
Venus	~3000	0.0041	$< 1 \times 10^{22}$
Earth	3486	1.003	8×10^{25}
Mars	~1700	0.975	$\lesssim 2.5 \times 10^{22}$
Jupiter	~52,000	2.44	1.55×10^{30}
Saturn	~28,000	2.39	5×10^{28}

†Adapted from Russell, C. T. (1980) *Rev. Geophys. Space Phys.* 18: 101.

internal dipole field *were* responsible, no external field should be present, since a dipolar-magnetized shell in theory does not produce an external magnetic field [89, 90]. Of course, craters and multi-ring basins produce anomalies in this ideal situation, but the strength of the field appears high enough to make the operation of a presently active dynamo, and hence a present fluid core, a distinct possibility [64].

The probable radius of the Mercurian core is about 1800 km. Mars is predicted to have a core of about the same size. The rotation period of Mars is close to that of the Earth, whereas the rotation period of Mercury is 59 days. Accordingly, conditions for the existence of a currently active dynamo on Mars should be more favorable than on Mercury but there is considerable controversy over the size of the magnetic moment of Mars, or whether it is, in fact, detectable at present [64, 92]. The solar wind apparently impinges on the Martian ionosphere.

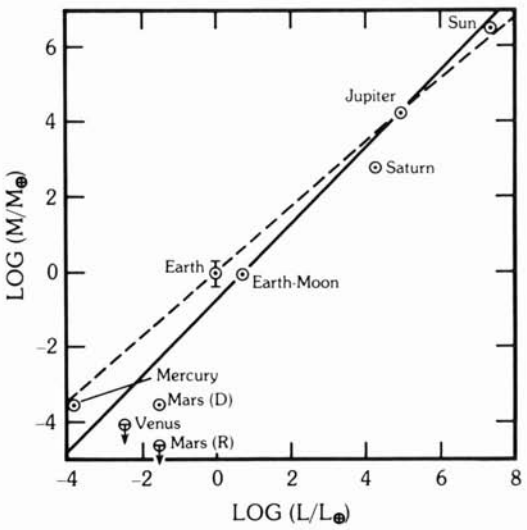

7.9 The magnetic moment of the planets and of the sun plotted against angular momentum. Both quantities are normalized to Earth. This is a magnetic version of Bode's Law [63]. Use of both the Earth and the Earth-Moon angular momentum results in two possible relationships.

Venus, which is a little smaller than the Earth, is thought to possess a core of about the same size. The rotation is retrograde with a period of 243 days, about four times that of Mercury. The large size of the core should produce a weak, but measurable field. No field has been detected, providing yet another instance of the difference between Venus and the Earth. Possibly the motions in the core, if it is liquid, are not sufficient to drive a dynamo. The absence of the magnetic field allows the solar wind to interact with the ionosphere, as is the situation with respect to Mars. It would be of interest to discover how long the surfaces of these two planets have been exposed to the solar wind. Figure 7.9 shows the correlation between angular momentum and magnetic moments of the sun and the planets.

Early magnetic fields recorded in the meteorites [93–97] are not discussed in this review. It should be noted that attempts to relate the lunar field to the presumed interplanetary field, responsible for the fossil magnetism observed in meteorites, may be misleading. Among other caveats, the fields responsible for the magnetic effects in meteorites were in existence about a billion years earlier than those responsible for the lunar magnetism [96]. Whether strong early magnetic fields were present is still not settled from the meteoritic evidence.

References and Notes

1. Coleman, P. J. (1979) *Science*. 205: 1082.
2. Lambeck, K. (1979) *JGR*. 84: 6241.
3. Bills, B. G., and Ferrari, A. J. (1977) *Icarus*. 31: 244.
4. El-Baz, F. (1973) *Science*. 180: 1173.
5. Mohan, S. N. (1979) *Icarus*. 38: 317.
6. Phillips, R. J., et al. (1981) *Science*. 212: 879.
7. Ananda, M. P., et al. (1977) *Moon*. 17: 101.
8. Kaula, W. M. (1979) *GRL*. 6: 191.
9. *Basaltic Volcanism* (1981) Section 4.2.1.
10. Kaula, W. M., et al. (1972) *PLC 3*: 2189; (1974) *PLC 5*: 3049.
11. Core offset was suggested by Ransford, G., and Sjogren, W. L. (1972) *Nature*. 238: 260. Kobrick, M. (1976) *Moon*. 15: 83, suggested random density anomalies would explain the effect.
12. Pullan, S., and Lambeck, K. (1980) *PLC 11*: 2031.
13. Wasson, J. T., and Warren, P. H. (1980) LPS XI: 1220.
14. Haines, E. L., and Metzger, A. E. (1980) *PLC 11*: 689.
15. Wood, J. A. (1973) *Moon*. 8: 73.
16. Phillips, R. J., and Lambeck, K. (1980) *Rev. Geophys. Space Phys*. 18: 27.
17. Muller, P. M., and Sjogren, W. L. (1968) *Science*. 161: 680.
18. Ferrari, A. J., et al. (1978) *JGR*. 83: 2863; compare Sjogren, W. L., et al. (1974) *Moon*. 11: 41.
19. Bills, B. G., and Ferrari, A. J. (1980) *JGR*. 85: 1013; Ferrari, A. J. (1975) *Science*. 188: 1297.
20. Phillips, R. J., and Dvorak, J. (1981) *Multi-ring Basins*, p. 91.

21. Arkani-Hamed, J. (1973) *PLC 4*: 2673.
22. See Chapter 3.
23. Dvorak, J., and Phillips, R. J. (1978) *PLC 9*: 3651.
24. Muller, P. M., et al. (1974) *Moon*. 10: 195; Scott, D. H. (1974) *PLC 5*: 3025.
25. Melosh, J. (1978) *PLC 9*: 3513; Solomon, S. C., and Head, J. W. (1979) *JGR*. 84: 1667; (1980) *Rev. Geophys. Space Phys*. 18: 107.
26. Lucchitta, B. K., and Watkins, J. A. (1978) *PLC 9*: 3459.
27. Pullan, S., and Lambeck, K. (1981) *PLC 12*: 853; Golombek, M. P. (1979) *JGR* 84: 4651.
28. Blasius, K. R., and Cutts, J. A. (1981) *Icarus*. 45: 87.
29. Smith, J. E., et al. (1980) NASA TM 81776, 79.
30. Comer, R. P., and Solomon, S. C. (1981) LPS XII: 166.
31. *Basaltic Volcanism* (1981) Section 4.5.5.
32. This corresponds to high values of the seismic parameter Q, which has typical values in the range 10–300 for the Earth, but is an order of magnitude higher (3000–5000) for the Moon. Values up to 5000 are given for the upper 5 km. See Tittmann, B. R., et al. (1979) *PLC 10*: 2131.
33. Latham, G., et al. (1973) *PLC 4*: 2518.
34. Kovach, R. L., and Watkins, J. S. (1973) *PLC 4*: 2550; Watkins, J. S., and Kovach, R. L. (1973) *PLC 4*: 2561.
35. Dainty, A. M., et al. (1974)*PLC 5*: 3091; Toksöz, M. N., et al. (1973) *PLC 4*: 2529; (1977) *Science*. 196: 979.
36. Nakamura, Y., et al. (1974) *PLC 5*: 2883; (1978) *PLC 9*: 3589; (1979) *PLC 10*: 2299.
37. Lazarewicz, A. R., et al. (1981) NASA Contractor Report 3408; Goins, N. E., and Lazarewicz, A. R. (1979) *GRL*. 6: 368.
38. Anderson, D. L., et al. (1977) *JGR*. 82: 4524.
39. Peeples, W. J., et al. (1978) *JGR*. 83: 3459.
40. Goins, N. R., et al. (1979) *PLC 10*: 2421; (1981) *JGR*. 86: 5061.
41. Nakamura, Y., et al. (1977) *PLC 8*: 487; *JGR*. 81: 4818.
42. Cleary, J. R. (1982) *JGR*. In press.
43. Hood, L. L., et al. (1981) LPS XII: 457.
44. Russell, C. J., et al. (1981) LPS XII: 914.
45. Solomon, S. C. (1979) *PEPI*. 19: 168.
46. Stevenson, D. J., and Yoder, C. F. (1981) LPS XII: 1043.
47. Brett, R. (1973) *GCA*. 37: 165; Goldstein, B. E., and Phillips, R. J. (1976) *PLC 7*: 3321.
48. Levin, B. J. (1979) *PLC 10*: 2321.
49. Langseth, M. G., et al. (1976) *PLC 7*: 3143.
50. Keihm, S. J., and Langseth, M. G. (1977) *PLC 8*: 499.
51. Sonett, C. P., et al. (1971) *Nature*. 230: 359; (1972) *PLC 3*: 2309.
52. Dyal, P., and Parkin, C. W. (1973) *PEPI*. 7: 251.
53. Dyal, P., et al. (1974) *PLC 5*: 3059.
54. Dyal, P., et. al. (1976) *PLC 7*: 3077; (1977) *PLC 8*: 767.
55. Vanyan, P. (1980) *Geophys. Surveys*. 4: 173.
56. Huebner, J. S., et al. (1979) *JGR. 84*: 4652; Hobbs, B. A. (1977) *Geophys. J. Roy Astr. Soc*. 51: 727.
57. Herbert, F., et al. (1981) LPS XII: 436; Hood, L. L., et al. (1981) LPS XII: 457.
58. Toksöz, M. N., et al. (1978) *Moon and Planets*. 18: 281.
59. Lambeck, K., and Pullan, S. (1980) *PEPI*. 22: 12.
60. Duba, A., et al. (1976) *PLC 7*: 3173.
61. Arkani-Hamed, J. (1974) *PLC 5*: 3127.